# Extended imaging, deconvolution, and two-way wavefields: a comparison

Esteban Díaz, Satyan Singh, and Paul Sava

**ABSTRACT**

Multiple-scattered waves contain information that is commonly disregarded during imaging and tomography. Marchenko wavefields are superior to time-reverse wavefields by handling primaries together with internal and surface-related multiples. Using all types of waves for imaging can greatly improve the illumination and augment the sensitivity of the data to errors in the background velocity model. We compare extended images computed with reverse time and Marchenko wavefields, and investigate the potential of using multidimensional deconvolution for extended images in order to obtain higher image resolution. Our experiments show that the Marchenko wavefields are sensitive to errors in the background model in a way that is similar to the sensitivity of time-reverse wavefields. The main difference between these imaging strategies is the improved angle illumination with the Marchenko wavefields due to the correct use of multiples; this improvement can eliminate the bias of tomography operators towards lower velocities when the data are contaminated with multiples.

**Key words:** extended imaging, deconvolution, multiples

## 1 INTRODUCTION

The quality of the seismic image depends on the choice of wave propagator, but more importantly on the quality of the background model. The better the velocity, the more focused the seismic image becomes. One can update the background velocity model in such a way that the image quality improves. By increasing the seismic image focusing, one effectively improves the synchronization of the source and receiver wavefields at the image locations. Image focusing can be observed in zero-offset sections by measuring the continuity and image strength, or by analyzing the focusing of point diffractors. However, if the events in the image consist mostly of continuous reflectors (layers inside the earth), the assessment of the background model accuracy becomes difficult. In order to retrieve the information about the kinematic error, one must extend the image away from zero offset, which allows to interpret the image at different points of view. In the context of two-way operators, the extension is usually performed by extended correlation in the image domain (Rickett and Sava, 2002; Sava and Fomel, 2006; Sava and Vasconcelos, 2011a), in the angle domain (Sava and Fomel, 2003; Yoon et al., 2004; Jin et al., 2014; Yoon et al., 2011; Vyas et al., 2011), or in the surface offset domain (Giboli et al., 2012). Once a suitable extension is chosen, the velocity error information can be extracted (1) by measuring focusing in the extended gathers (Shen and Symes, 2008; Weibull and Arntsen, 2013; Yang et al., 2013; Shan and Wang, 2013; Biondi and Almomin, 2014; Díaz and Sava, 2015; Yang and Sava, 2015), (2) by measuring moveout in the angle or surface offset gathers (Liu and Han, 2010; Shen et al., 2015; Fleury et al., 2014), (3) or by measuring the consistency between individual shot record images (Perrone et al., 2015).

Another important factor that determines the quality of a seismic image is the amount of data illuminating a target in the subsurface. Great effort is invested in bigger acquisition campaigns to increase the illumination of a seismic target. Most of the current imaging (and modeling) technologies utilize the primaries in the data but disregard the multiples. By utilizing the multiples one can better illuminate the targets with smaller acquisition campaigns (Verschuur and Berkhout, 2011). In order to incorporate the multiples into the seismic images, a conventional approach is to use the primaries as an areal source for the surface-related multiples; this allows one to image the first order surface-related multiples in the same position as the primaries (Guitton, 2002; Grion et al., 2007; Verschuur and Berkhout, 2011; Whitmore et al., 2010; Wong et al., 2015). However, these techniques require prior separation of multiples and primaries. A recent alternative to incorporate the multiples into the imaging process is the Marchenko modeling framework in which the multiples are used together with the primaries in a global prediction procedure to find focusing solutions that, when injected into the surface, produce wavefield focusing at an arbitrary location in the subsur-

face (Broggini and Snieder, 2012; Behura et al., 2014; Wapenaar et al., 2014b; Singh et al., 2015). The focusing solutions are guaranteed to exist regardless of the background velocity model. Once the focusing functions are found the up- and down-going Green's functions are computed through convolutions and correlations between the focusing solutions and the surface data. The method was initially developed to handle internal multiples (Broggini and Snieder, 2012; Behura et al., 2014; Wapenaar et al., 2014b) and was later extended to incorporate surface-related multiples (Singh et al., 2015) .

In this article, we show sensitivity of the Marchenko wavefields to the background model which is similar to conventional one-way or RTM wavefields. We assess the sensitivity by using extended images and compare the moveout with conventional RTM extended images. We pose the extended imaging process as an inversion problem which can be thought of as an extended deconvolution imaging condition. Assessing the sensitivity to errors in the background is the first step towards the formulation of a tomographic problem. Furthermore, Marchenko wavefields can eliminate the need for the separation of primaries and multiples in tomography, and increase the illumination of the subsurface targets.

This paper is organized as follows: first, we establish some differences and similarities between conventional two-way RTM operators and Green's function retrieval with Marchenko; next, we review the extended imaging and deconvolution process; and finally, we show examples comparing the sensitivity of RTM and Marchenko modeling approaches to the background model.

## 2 MODELING DIFFERENCES

In this section, we review similarities and differences between Marchenko and RTM propagators. While both propagators are two-way, Marchenko separates the total wavefield $u$ into up- and down-going components:

$$u(\mathbf{x}, \mathbf{x}_s, t) = u_s(\mathbf{x}, \mathbf{x}_s, t) + u_r(\mathbf{x}, \mathbf{x}_s, t). \tag{1}$$

This separation is necessary because the method relies on one-way reciprocity theorems (Wapenaar et al., 2014a). Singh et al. (2015) show how to recover the total wavefield $u$, and its directional components $u_s$ and $u_r$ with a free-surface condition which allows to correctly model primaries, internal multiples, and surface-related multiples.

The algorithm in Singh et al. (2015) finds the focusing solutions $f_1^+(\mathbf{x}_s, \mathbf{x}, t)$ and $f_1^-(\mathbf{x}_s, \mathbf{x}, t)$ which produce a focus at an arbitrary location $\mathbf{x}$ in the subsurface by injection at the surface at coordinates $\mathbf{x}_s$. The focusing solutions always exist regardless the background model. In order to obtain the focusing solutions, the method utilizes the recorded data $R(\mathbf{x}_s, \mathbf{x}_r, t)$ together with an estimate of the direct arrival $T_d(\mathbf{x}, \mathbf{x}_r, t)$ which goes from the subsurface point $\mathbf{x}$ to the surface locations $\mathbf{x}_r$. The direct arrival information contains embedded the kinematic information from the background model. If the direct arrival information is accurate, the recovered wavefield satisfies the wave equation

$$\rho\nabla\cdot\left(\frac{1}{\rho}\nabla u\right) + \frac{\omega^2}{v^2}u = -j\omega\rho\delta(\mathbf{x}-\mathbf{x}_s) \tag{2}$$

for a volumetric injection source $-j\omega\rho\delta(\mathbf{x}-\mathbf{x}_s)$, density $\rho$, and velocity $v$ from the true medium. If the direct arrival information $T_d$ is obtained from a wrong background velocity model, the retrieved wavefield is a representation of the true Green's function with the kinematics of the background model.

Once the focusing functions are computed through the iterative scheme described in Singh et al. (2015), the individual wavefield components are obtained through the following equations (Singh et al., 2015):

$$u_r(\mathbf{x}, \mathbf{x}_r, \omega) = -f_1^-(\mathbf{x}_r, \mathbf{x}, \omega) + \tag{3}$$
$$\sum_{\mathbf{x}_s} f_1^+(\mathbf{x}_s, \mathbf{x}, \omega)\, R(\mathbf{x}_r, \mathbf{x}_s, \omega) - r f_1^-(\mathbf{x}_s, \mathbf{x}, \omega)\, R(\mathbf{x}_r, \mathbf{x}_s, \omega),$$

$$u_s(\mathbf{x}, \mathbf{x}_r, \omega) = +f_1^+(\mathbf{x}_r, \mathbf{x}, \omega)^* - \tag{4}$$
$$\sum_{\mathbf{x}_s} f_1^-(\mathbf{x}_s, \mathbf{x}, \omega)^*\, R(\mathbf{x}_r, \mathbf{x}_s, \omega) - r f_1^+(\mathbf{x}_s, \mathbf{x}, \omega)\, R(\mathbf{x}_r, \mathbf{x}_s, \omega).$$

Note that the inputs for computing either wavefield are the same: the focusing solutions $f_1^+$ and $f_1^-$, the data at the surface $R$, and the reflection coefficient at the free surface $r = -1$. The focusing solutions $f_1^-$ and $f_1^+$ can be thought of as the propagators that redatum the data from the source position $\mathbf{x}_s$ to the image point $\mathbf{x}$.

In contrast, the RTM propagators obtain the source and receiver wavefields through two independent modeling problems:

$$L(v)u_s = f_s, \tag{5}$$

which is solved forward in time for the source function $f_s$, and

$$L^\top(v)u_r = f_r, \tag{6}$$

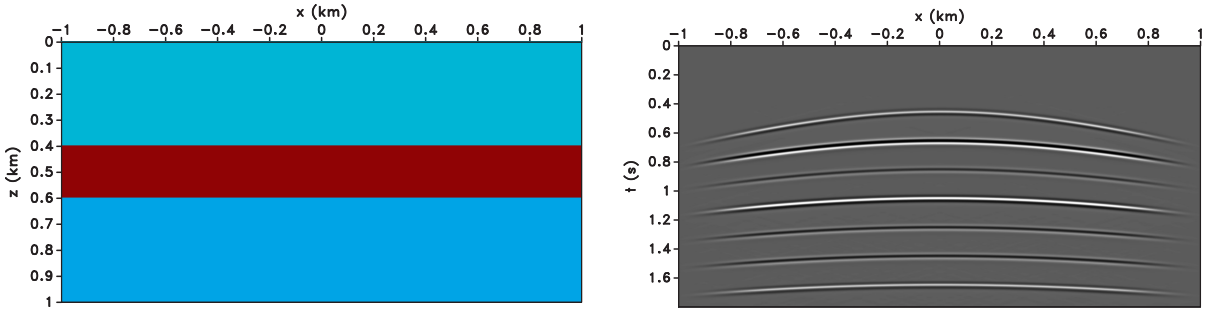
which is solved backward in time for the receiver data $f_r = \sum_{\mathbf{x}_r} R(\mathbf{x}_s, \mathbf{x}_r, t)\delta(\mathbf{x}-\mathbf{x}_r)$. Note that for the RTM propagators, the sum of the source and receiver wavefields does not satisfy equation 2 and does not handle correctly the multiples present in the data.

## 3 SENSITIVITY TO THE BACKGROUND MODEL

In the Marchenko context, the wavefield $u_r$ represents the upgoing component of the Green's function, whereas $u_s$ represents the downgoing component. Following the imaging principle (Claerbout, 1971) the image $I(\mathbf{x})$ is constructed when wavefields $u_s$ and $u_r$ coincide in space and time:

$$I(\mathbf{x}) = \sum_{\mathbf{x}_s, t} u_s(\mathbf{x}_s, \mathbf{x}, t) u_r(\mathbf{x}_s, \mathbf{x}, t). \tag{7}$$

Although helpful for understanding the subsurface, $I(\mathbf{x})$ does not contain much information about the quality of the background velocity model. Instead, one can use the extended imaging condition (Rickett and Sava, 2002; Sava and Fomel,




(a) (b)

**Figure 1.** Free surface experiment with a constant velocity background: (a) variable density model and (b) the recorded data for a shot at $\mathbf{x}_s = (0, 0)$km. Note how the data contain primaries (first two arrivals), internal multiples (weak third arrival), and the corresponding surface-related multiples.

2003; Sava and Vasconcelos, 2011b) to analyze the interaction between source and receiver wavefields at the vicinity of the image location $\mathbf{x}$ and $t = 0$:

$$I(\mathbf{x}, \boldsymbol{\lambda}, \tau) = \sum_{\mathbf{x}_s, t} u_s(e, \mathbf{x} - \boldsymbol{\lambda}, t - \tau) u_r(e, \mathbf{x} + \boldsymbol{\lambda}, t + \tau), \quad (8)$$

where $\boldsymbol{\lambda}$ and $\tau$ are the space- and time-lags of the correlation, respectively. The extended-imaging operator is linear and represents the down-going field, $u_s$, interacting with the up-going field, $u_r$; which in matrix-vector can be written as

$$I = \mathbf{U_s}^\top u_r, \quad (9)$$

where, the matrix $\mathbf{U_s}^\top$ is the extended-imaging operator applied to the receiver field $u_r$. Alternatively, one can think about the (extended) imaging process as an inversion problem such that $I(\mathbf{x}, \boldsymbol{\lambda}, \tau)$ satisfies the relation

$$\mathbf{U_s} I \approx u_r, \quad (10)$$

where the operator $\mathbf{U_s}$ implements:

$$\tilde{u_r}(\mathbf{x}_s, \mathbf{x}, t) = \sum_{\tau, \boldsymbol{\lambda}} I(\mathbf{x} - \boldsymbol{\lambda}, \boldsymbol{\lambda}, \tau) u_s(\mathbf{x}_s, \mathbf{x} - 2\boldsymbol{\lambda}, t + 2\tau). \quad (11)$$

The wavefield $\tilde{u_r}$ denotes the action of $\mathbf{U_s}$ applied to $I$. The relation in equation 10 implies that the extended reflectivity $I(\mathbf{x}, \boldsymbol{\lambda}, \tau)$ is the ratio between the down- and up-going fields at the surrounding locations of image point $\mathbf{x}$ and around time $t = 0$. In order to stabilize the inversion, one can also add a damping goal by trying to keep the extended reflectivity as small as possible:

$$\epsilon I \approx 0. \quad (12)$$

The composite system can be written as

$$\left(\mathbf{U_s}^\top \mathbf{U_s} + \epsilon^2 \mathbf{I}\right) I = \mathbf{U_s}^\top u_r, \quad (13)$$

and can be solved with a linear conjugate gradient algorithm. Note that the matrix $\mathbf{U_s}^\top \mathbf{U_s}$ does not need to be formed; instead one needs to compute the action of the matrix to the input reflectivity $I(\mathbf{x}, \boldsymbol{\lambda}, \tau)$. The deconvolution process is similar to the one discussed by Valenciano et al. (2009) and is also referred to as multi-dimensional deconvolution (MDD) by van der Neut et al. (2011). Both, extended correlation and deconvolution images contain kinematic information about the quality of the background model. However, the latter is a better approximation of the reflectivity and is better focused.

## 4 EXAMPLES

In this section, we compare the behavior of RTM and Marchenko wavefields for finding errors in the background velocity model. We use a simple 1D model with a constant background velocity and a variable density profile depicted in Figure 1(a). The pressure data are generated with a free-surface boundary condition shown in Figure 1(b). The main objective of this exercise is to investigate the sensitivity of the Marchenko images to errors in the background model, which is the first step towards a formulation of a tomography problem.

We use the subset of the extended image with $\tau = 0$, i.e. space-lag gathers, at $x = 0$ for a slow, correct, and fast constant background velocities. Figures 2(a)-2(c) show the gathers computed using the conventional RTM propagator, where one can observe the strong response of the multiples present in the data. Among all of the reflectors present in the gather, only the first two correspond to the true interfaces; the rest correspond to misplaced surface-related events. Figures 2(d)-2(f) show the corresponding common angle gathers for slow, correct, and fast models, respectively. The transformation from space-lag $\boldsymbol{\lambda}$ to angle $\theta$ is described in Sava and Fomel (2006). For this particular model, the velocity is constant; hence, the reflection coefficient should remain constant as a function of the scattering angle. We recompute the same set of images with the deconvolution framework in equation 13: Figures 3(a)-3(c) show the deconvolved space-lag gathers with RTM wavefields, and Figures 3(d)-3(f) show the corresponding angle gathers with the RTM wavefields. In these figures, the amplitudes across angles are more evenly distributed. The deconvolved space-lag gathers contain more energy at larger lags; this can be beneficial for improved tomographic updates because during tomog-

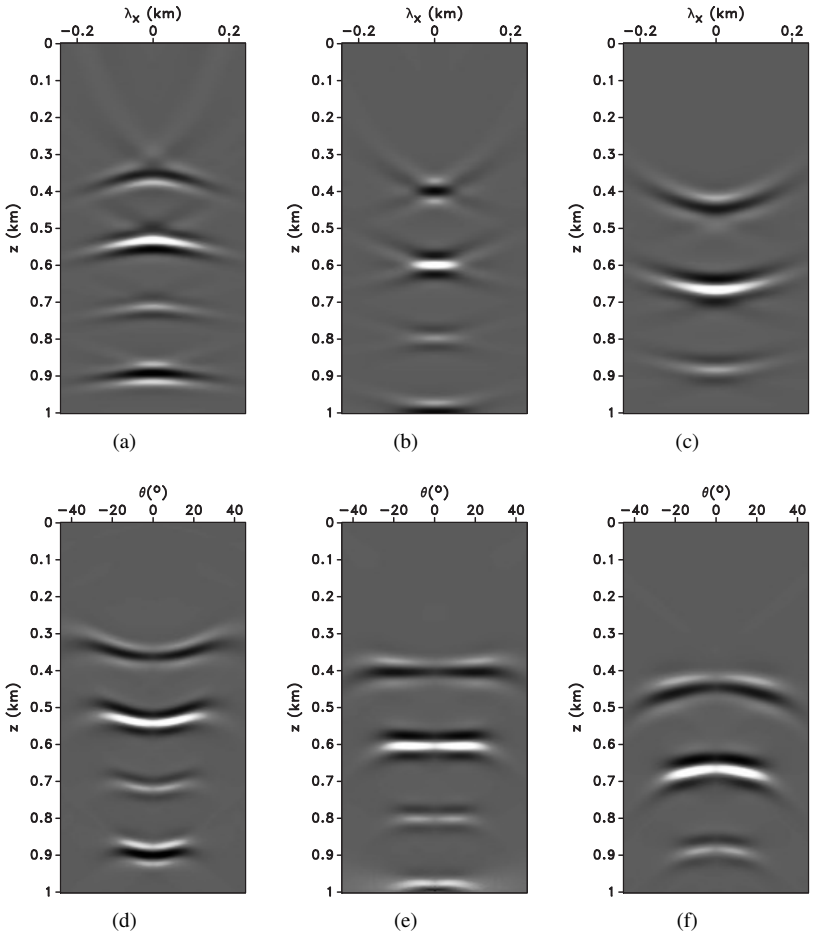



**Figure 2.** The top row shows space-lag gathers obtained from RTM wavefields for (a) low, (b) correct, and (c) fast velocity. The bottom row shows the corresponding angle gathers for (d) low, (e) correct, and (f) fast velocity.

raphy, the objective function measures the energy away from $\boldsymbol{\lambda} = 0$ (Shen and Symes, 2008):

$$J = ||\boldsymbol{\lambda} I(\mathbf{x}, \boldsymbol{\lambda})||_2^2 \,. \tag{14}$$

Hence, by using deconvolution, one can better highlight aspects of the gathers that need improvement through changes to the velocity.

We repeat the same experiment using the Marchenko wavefields. Figures 4(a)-4(c) show the space-lag gathers for low, correct, and fast background velocity, respectively. The main difference between these gathers and those in Figures 2(a)-2(c) is the correct handling of the surface-related and internal multiples. Despite the characteristics of the method, where the focusing solutions $f_1^+$ and $f_1^-$ always exist, the gathers present moveout, indicating errors in the background model. Also, the focusing for the correct velocity model, Figure 4(b), is improved when compared to Figure 2(b). This enhancement in focusing is due to the improved illumination achieved by incorporating surface-related and internal multiples in the final image, which implies that one effectively increases the aperture with depth. In the conventional imaging we see misplaced events due to multiples; similarly, with Marchenko wavefields, we can identify events above the true interfaces. Such events are caused by the interaction of multiples in the source wavefield with primaries in the receiver wavefield. However, these events are very weak as shown in the Marchenko gathers. The angle gathers from Figures 4(d)-4(f) show a stronger response in the near angles, which shows the added illumination from internal and surface-related multiples. After deconvolving the Marchenko gathers (Figures 5(a)-5(c)) , the focus greatly improves, which can be better appreciated with the correct velocity case, Figure 5(b). We also see the same pattern as with Figures 3(a)-3(c) where the energy spreads more evenly over space-lags. The angle gathers (Figures 5(d)-5(f)) show a better amplitude distribution with angle. Also the angle range illuminated with the Marchenko fields remains somewhat constant with depth, whereas the angle gathers with conventional fields decrease the angle illumination with depth. This can have great impact on tomography where, with conventional propagators, the uncertainty increases rapidly in poorly illuminated areas.

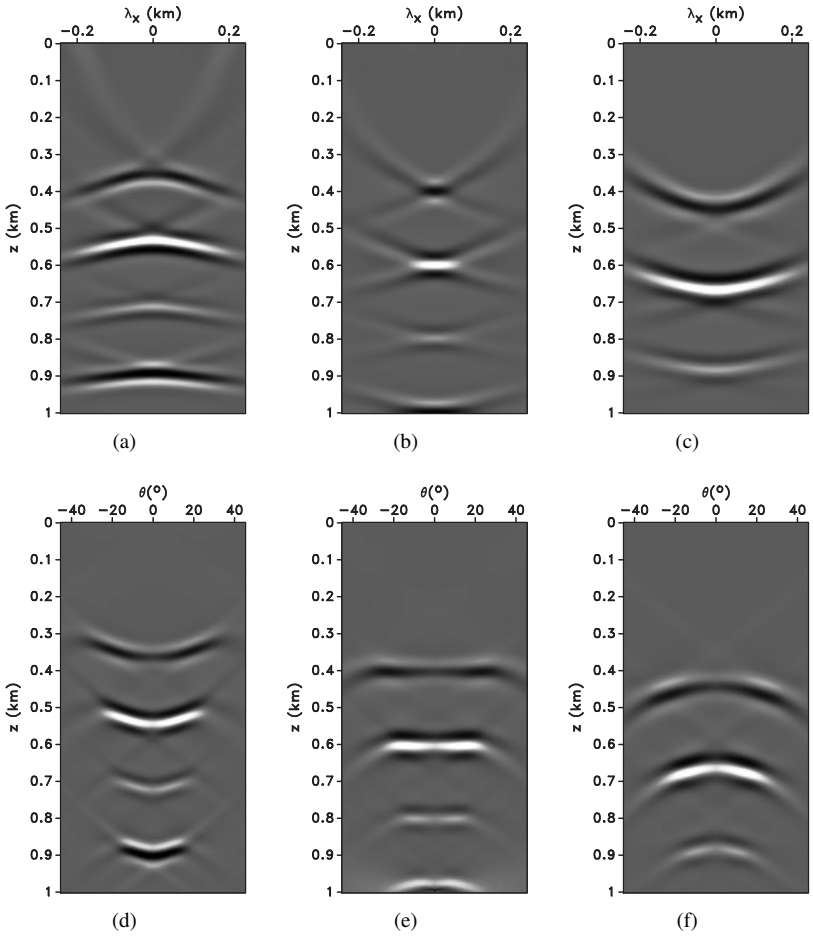



**Figure 3.** The top row shows deconvolved space-lag gathers obtained from RTM wavefields for (a) low, (b) correct, and (c) fast velocity. The bottom row shows the corresponding deconvolved angle gathers for (d) low, (e) correct, and (f) fast velocity.

### 4.1 Sigsbee model

In this example, we use a subset of the Sigsbee model (Paffenholz et al., 2002) from the sediment section, shown in Figure 6. Using a free-surface boundary condition we generate shot gathers at the surface with a bandpass wavelet with a high-cut of $50$Hz. We compute extended images from Marchenko wavefields for low, correct, and high velocity models that are obtained by scaling the correct model by $0.9$, $1.0$, and $1.1$, respectively. For the three models, we compute conventional and deconvolved extended images; for each case, we show the corresponding angle gathers along the section. The angle range for each gather spans from $\theta = [-45, 45]^o$.

Figures 7(a), 7(c), and 7(e) depict the angle gathers from the Marchenko wavefields for low, correct, and fast velocity models, respectively. Note that the angle gathers do not contain visible artifacts from multiples in the data. Similarly to the simple example from the preceding section, the angle gathers show moveout that is indicative of the errors in the background model, in a similar way as conventional RTM gathers. Figures 7(b), 7(d), and 7(f) show the corresponding angle gathers after the extended deconvolution process. The improved angle illumination can be seen when the amplitude is better balanced across angles, in a similar way as the previous example. An area of such improvement is at around $z = 0.5$km, where the illumination increases at near and mid angles.

## 5 CONCLUSIONS

We compare image gathers obtained with Marchenko and RTM propagators. The Marchenko gathers correctly image primaries, internal multiples, and surface-related multiples. It also produces weak events above the correct interface depth due to the interaction of primaries with the surface-related multiples. In contrast, RTM gathers treat the multiples as primaries; hence, the events are imaged in the wrong location and can bias an inversion towards lower velocities. The Marchenko and RTM gathers show similar sensitivity to errors in the background model. However, the Marchenko gathers possess increased illumination due to increased effective aperture, as shown by the angle gathers in our experiments. We also show

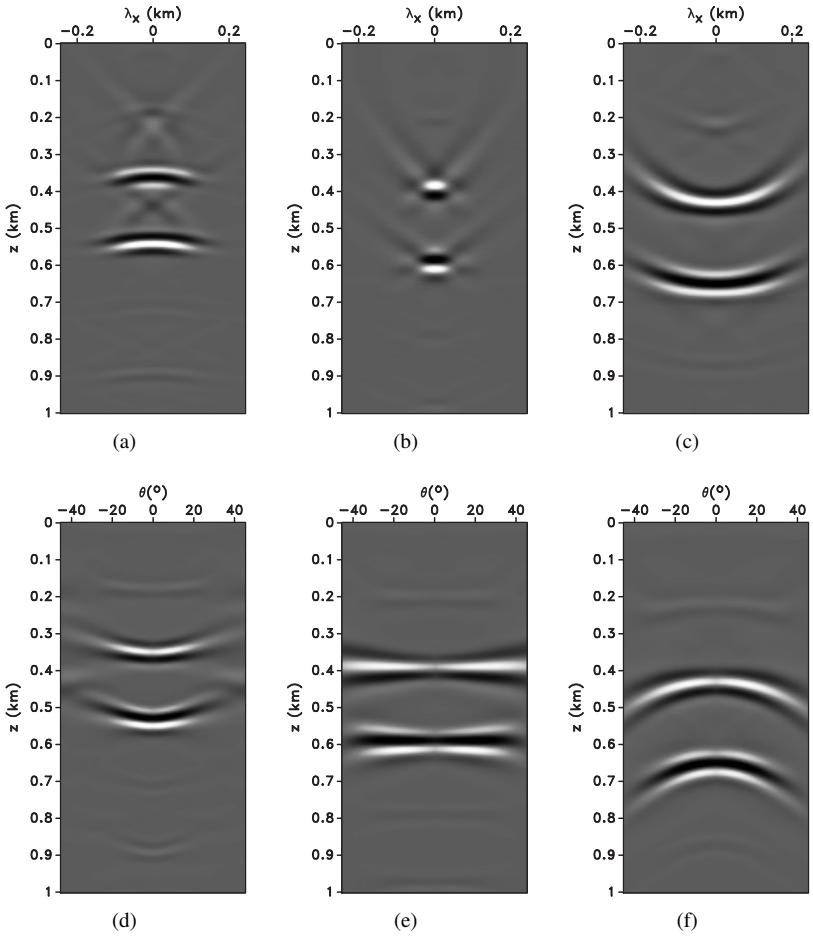



**Figure 4.** The top row shows space-lag gathers obtained from Marchenko wavefields for (a) low, (b) correct, and (c) fast velocity. The bottom row shows the corresponding angle gathers for (d) low, (e) correct, and (f) fast velocity.

the benefits of posing the extended imaging as a deconvolution problem instead of correlation. The gather focus improves, and the energy distribution is more homogeneous as a function of angle. The use of Marchenko wavefields together with extended deconvolution can benefit tomography operator. The dependency of the Marchenko wavefield with respect to the background velocity model is not as explicit as with the RTM wavefields. In Marchenko modeling, the kinematics are embedded in the direct arrival information used as input for the framework. The most appropriate method to update the background model is a subject for current and future research.

## 6 ACKNOWLEDGMENTS

We thank the sponsors of the Center for Wave Phenomena, whose support made this research possible. The reproducible numeric examples in this paper use the Madagascar open-source software package (Fomel et al., 2013) freely available from http://www.ahay.org.

## REFERENCES

Behura, J., K. Wapenaar, and R. Snieder, 2014, Autofocus imaging: Image reconstruction based on inverse scattering theory: Geophysics, **79**, A19–A26.

Biondi, B., and A. Almomin, 2014, Simultaneous inversion of full data bandwidth by tomographic full-waveform inversion: Geophysics, **79**, WA129–WA140.

Broggini, F., and R. Snieder, 2012, Connection of scattering principles: a visual and mathematical tour: European Journal of Physics, **33**, 593.

Claerbout, J. F., 1971, Toward a unified theory of reflector mapping: Geophysics, **36**, 467–481.

Díaz, E., and P. Sava, 2015, Wavefield tomography using reverse time migration backscattering: Geophysics, **80**, R57–R69.

Fleury, C., M. Giboli, and R. Baina, 2014, Moveout analysis for reflection tomography on wave-equation image gathers: SEG Technical Program Expanded Abstracts 2014, 4788–4792.

Fomel, S., P. Sava, I. Vlad, Y. Liu, and V. Bashkardin, 2013,

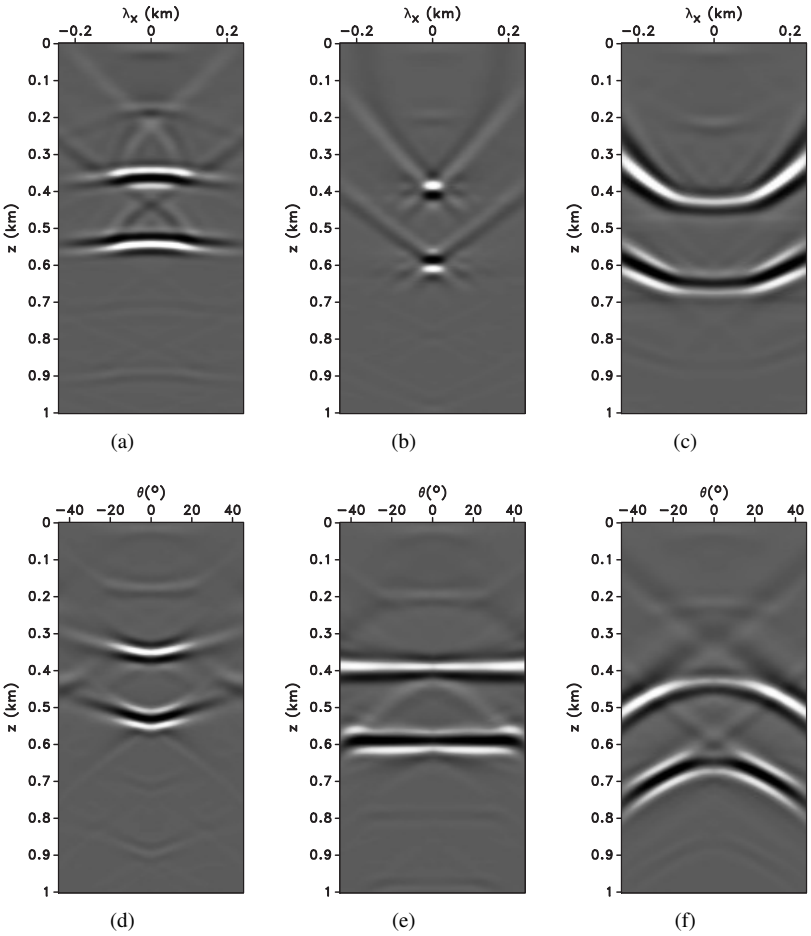



**Figure 5.** The top row shows deconvolved space-lag gathers obtained from Marchenko wavefields for (a) low, (b) correct, and (c) fast velocity. The bottom row shows the corresponding deconvolved angle gathers for (d) low, (e) correct, and (f) fast velocity. Note how the amplitude distribution is more homogeneous for the deconvolved angle gathers, also the focus for the correct velocity is much better than Figure 4(b).

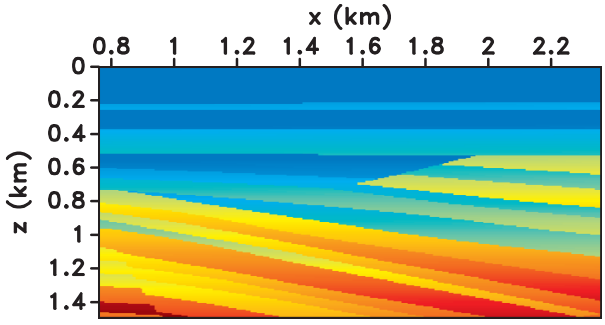



**Figure 6.** Subset from the sediment area of the Sigsbee model.

Madagascar: open-source software project for multidimensional data analysis and reproducible computational experiments: Journal of Open Research Software, **1**, e8.

Giboli, M., R. Baina, L. Nicoletis, and B. Duquet, 2012, Reverse time migration surface offset gathers part 1: a new method to produce classical common image gathers: 1–5.

Grion, S., R. Exley, M. Manin, X. Miao, A. Pica, Y. Wang, P. Granger, and S. Ronen, 2007, Mirror imaging of obs data: first break, **25**.

Guitton, A., 2002, Shotprofile migration of multiple reflec-

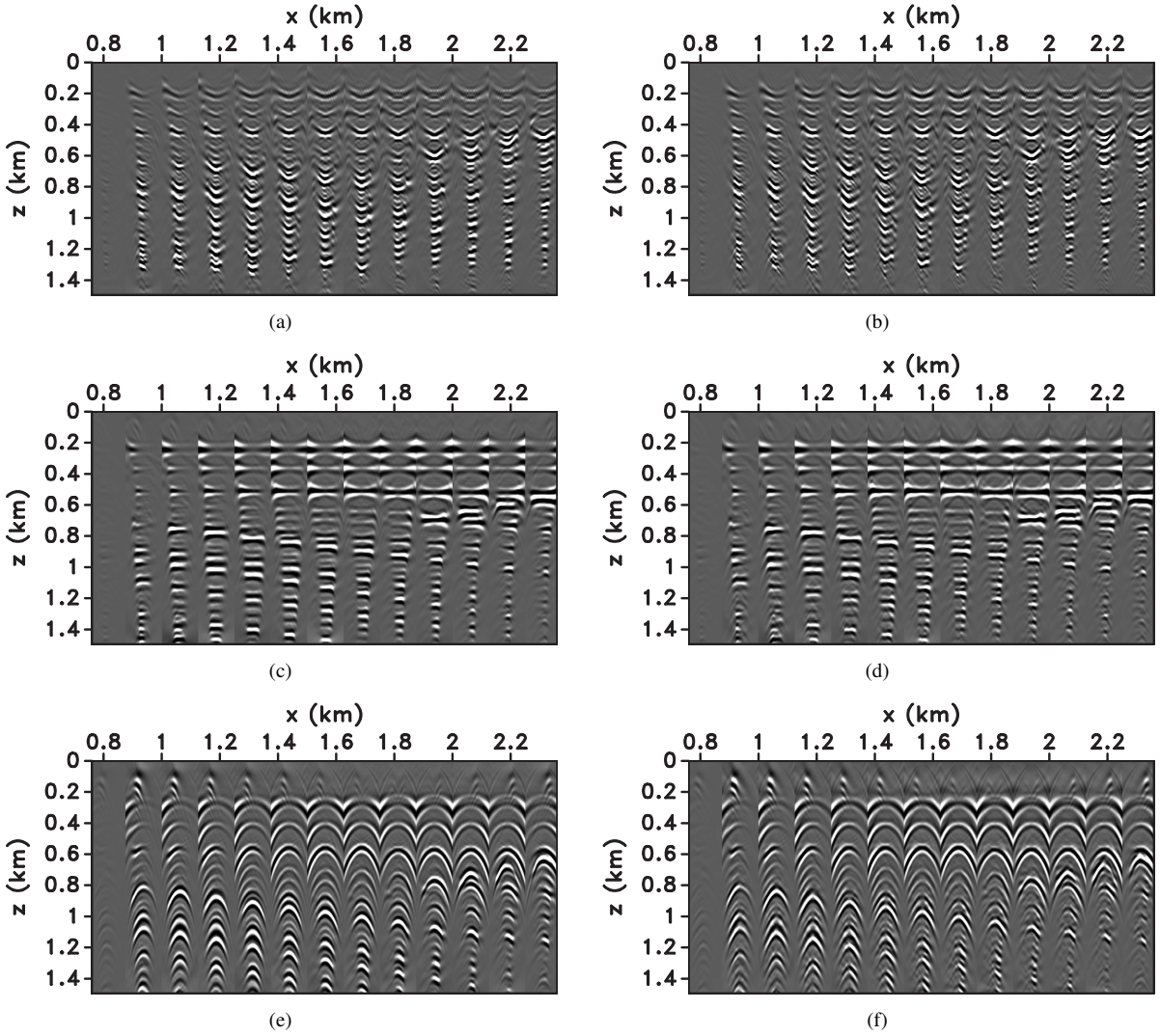



**Figure 7.** Retrieved Marchenko angle gathers obtained after mapping space-lag gathers to the angle domain. The left column shows the angle gathers transformed from extended images for (a) slow, (c) correct, and (e) fast model. The right column shows the angle gathers transformed from the deconvolved space-lag gathers for (b) slow, (d) correct, and (f) fast model. Note the improved response after the deconvolution process at near angles.

tions: SEG Technical Program Expanded Abstracts 2002, 1296–1299.

Jin, H., G. A. McMechan, and H. Guan, 2014, Comparison of methods for extracting adcigs from RTM: Geophysics, **79**, S89–S103.

Liu, J., and W. Han, 2010, Automatic event picking and tomography on 3d rtm angle gathers: 4263–4268.

Paffenholz, J., B. McLain, J. Zaske, and P. Keliher, 2002, Subsalt multiple attenuation and imaging: Observations from the sigsbee 2b synthetic dataset: 72nd Annual International Meeting, SEG, Expanded Abstracts, 2122–2125.

Perrone, F., P. Sava, and J. Panizzardi, 2015, Waveform tomography based on local image correlations: Geophysical Prospecting, **63**, 35–54.

Rickett, J. E., and P. C. Sava, 2002, Offset and angle-domain common image-point gathers for shot-profile migration: Geophysics, **67**, 883–889.

Sava, P., and S. Fomel, 2006, Time-shift imaging condition in seismic migration: Geophysics, **71**, S209–S217.

Sava, P., and I. Vasconcelos, 2011a, Extended imaging conditions for wave-equation migration: Geophysical Prospecting, **59**, 35–55.

———, 2011b, Extended imaging conditions for wave-equation migration: Geophysical Prospecting, **59**, 35–55.

Sava, P. C., and S. Fomel, 2003, Angle-domain common-image gathers by wavefield continuation methods: Geophysics, **68**, 1065–1074.

Shan, G., and Y. Wang, 2013, Rtm based wave equation mi-

gration velocity analysis: 4726–4731.
Shen, P., and W. W. Symes, 2008, Automatic velocity analysis via shot profile migration: Geophysics, **73**, VE49–VE59.
Shen, Y., B. Biondi, and R. Clapp, 2015, Wave-equation based q tomography from angle-domain common image gathers: 4334–4338.
Singh, S., R. Snieder, J. Behura, J. van der Neut, K. Wapenaar, and E. Slob, 2015, Marchenko imaging: Imaging with primaries, internal multiples, and free-surface multiples: Geophysics, **80**, S165–S174.
Valenciano, A. A., B. L. Biondi, and R. G. Clapp, 2009, Imaging by target-oriented wave-equation inversion: Geophysics, **74**, WCA109–WCA120.
van der Neut, J., J. Thorbecke, K. Mehta, E. Slob, and K. Wapenaar, 2011, Controlled-source interferometric redatuming by crosscorrelation and multidimensional deconvolution in elastic media: Geophysics, **76**, SA63–SA76.
Verschuur, D. J. E., and A. J. G. Berkhout, 2011, Seismic migration of blended shot records with surface-related multiple scattering: Geophysics, **76**, A7–A13.
Vyas, M., D. Nichols, and E. Mobley, 2011, Efficient RTM angle gathers using source directions: 3104–3108.
Wapenaar, K., J. Thorbecke, J. van der Neut, F. Broggini, E. Slob, and R. Snieder, 2014a, Green's function retrieval from reflection data, in absence of a receiver at the virtual source position: The Journal of the Acoustical Society of America, **135**, 2847–2861.
———, 2014b, Marchenko imaging: Geophysics, **79**, WA39–WA57.
Weibull, W., and B. Arntsen, 2013, Automatic velocity analysis with reverse-time migration: Geophysics, **78**, S179–S192.
Whitmore, N. D., A. A. Valenciano, W. Sollner, and S. Lu, 2010, Imaging of primaries and multiples using a dual-sensor towed streamer: SEG Technical Program Expanded Abstracts 2010, 3187–3192.
Wong, M., B. L. Biondi, and S. Ronen, 2015, Imaging with primaries and free-surface multiples by joint least-squares reverse time migration: Geophysics, **80**, S223–S235.
Yang, T., and P. Sava, 2015, Image-domain wavefield tomography with extended common-image-point gathers: Geophysical Prospecting, **63**, 1086–1096.
Yang, T., J. Shragge, and P. Sava, 2013, Illumination compensation for image-domain wavefield tomography: Geophysics, **78**, U65–U76.
Yoon, K., M. Guo, J. Cai, and B. Wang, 2011, 3D RTM angle gathers from source wave propagation direction and dip of reflector: SEG Technical Program Expanded Abstracts 2011, 3136–3140.
Yoon, K., K. J. Marfurt, and W. Starr, 2004, Challenges in reversetime migration: SEG Technical Program Expanded Abstracts, 1057–1060.